Collaborative Beamforming for Wireless Sensor Networks with Gaussian Distributed Sensor Nodes

Mohammed F. A. Ahmed, *Student Member, IEEE*, and Sergiy A. Vorobyov, *Senior Member, IEEE*

Abstract—Collaborative beamforming has been recently introduced in the context of wireless sensor networks (WSNs) to increase the transmission range of individual sensor nodes. The challenge in using collaborative beamforming in WSNs is the uncertainty regarding the sensor node locations. However, the actual sensor node spatial distribution can be modeled by a properly selected probability density function (pdf). In this paper, we model the spatial distribution of sensor nodes in a cluster of WSN using Gaussian pdf. Gaussian pdf is more suitable in many WSN applications than, for example, uniform pdf which is commonly used for *flat* ad hoc networks. The average beampattern and its characteristics, the distribution of the beampattern level in the sidelobe region, and the distribution of the maximum sidelobe peak are derived using the theory of random arrays. We show that both the uniform and Gaussian sensor node deployments behave qualitatively in a similar way with respect to the beamwidths and sidelobe levels, while the Gaussian deployment gives wider mainlobe and has lower chance of large sidelobes.

Index Terms—Ad hoc networks, sensor networks, antennas and propagation, resource allocation and interference management.

I. INTRODUCTION

WIRELESS sensor networks (WSNs) have recently become a practical technology and increasingly being introduced to different applications [1]. In many WSN applications, it is required to transmit the acquired data over long distances using transmission resources available only at sensor nodes. However, this can be power costly for individual sensor nodes due to their limited power resources [2]. The transmission range extension in WSNs can be achieved using collaborative beamforming [3], [4]. Specifically, WSN can be deployed in a form of disjointed sensor node clusters where all sensor nodes within one cluster act collaboratively as distributed antenna array. Each sensor node broadcasts its data to other sensor nodes in a cluster, and the same data symbols are transmitted by all sensor nodes synchronously. The individual signals from sensor nodes arrive in phase and constructively add at the intended destination which can be a neighboring cluster or a base station. Collaborative beamforming concentrates the radiation power in a certain direction and reduces the power lose in other directions. Moreover, collaborative

beamforming distributes power consumption over all sensor nodes.

The beampattern characteristics of collaborative beamforming have been recently derived in [3] using the random array theory (see [5], [6]), and assuming that sensor nodes in one cluster of WSN are uniformly distributed. However, the actual sensor node distribution depends on the deployment method. Indeed, to cover a wide area, large numbers of sensor nodes must be deployed simultaneously in an *ad hoc* way which cannot guarantee uniform distribution over the area. An example of such application is rural areas monitoring when the deployment is done by dropping a group of sensor nodes from an airplane. The spatial distribution of sensor nodes in this case is argued to be Gaussian [7] – [9]. Indeed, the sensor nodes actual locations are affected by different factors such as wind, the releasing mechanism, speed, height, etc. The displacement from the targeted location due to each of these multiple factors can be modeled as a random variable and the effective displacement is the sum of these random variables. Therefore, according to the central limit theorem, the actual location will follow Gaussian distribution.

In this paper, Gaussian probability density function (pdf) is used to model the spatial sensor node distribution in a cluster of WSN. The average beampattern and its characteristics are derived under this assumption. The distribution of the beampattern level in the sidelobe region and the distribution of the maximum sidelobe peak are also found. The beampattern characteristics derived in the case of Gaussian pdf are compared to the corresponding characteristics in the case of uniform spatial sensor node distribution.

II. AVERAGE BEAMPATTERN AND ITS CHARACTERISTICS

A. System model and beampattern definition

We consider the geometric model introduced in [3] for a cluster of N sensor nodes co-located in (x, y) plane. The rectangular sensor nodes coordinates (x_k, y_k), $k = 1, \ldots, N$, are chosen randomly according to Gaussian distribution with zero mean and variance σ_o^2. The corresponding spherical coordinates $\left(r_k = \sqrt{x_k^2 + y_k^2}, \ \psi_k = \tan^{-1}(\frac{y_k}{x_k}) \right)$ have Rayleigh and uniform distributions, respectively, i.e., $f_{r_k}(r) = \frac{r}{\sigma_o^2} \exp^{-\frac{r^2}{2\sigma_o^2}}, 0 \leq r < \infty$ and $f_{\psi_k}(\psi) = \frac{1}{2\pi}, -\pi \leq \psi < \pi$.

Let the destination base station be located in (x, y) plane at coordinates (A, ϕ_0). Without any loss of generality, we can set $\phi_0 = 0$. The Euclidean distance between the kth sensor node and a point (A, ϕ) is defined as $d_k(\phi) \triangleq \sqrt{A^2 + r_k^2 - 2r_k A \cos(\phi - \psi_k)} \approx A - r_k \cos(\phi - \psi_k)$, where $A \gg r_k$ in the far-field region. Introducing the location vectors $\mathbf{r} = [r_1, r_2, \ldots, r_N] \in [0, \infty)^N$ and $\boldsymbol{\psi} = [\psi_1, \psi_2, \ldots, \psi_N]$

$\in [-\pi, \pi)^N$ for a cluster of randomly located sensor nodes, the array factor can be defined as

$$F(\phi/\mathbf{r}, \boldsymbol{\phi}) = \frac{1}{N} \sum_{k=1}^{N} e^{j\varphi_k} e^{j\frac{2\pi}{\lambda} d_k(\phi)} \qquad (1)$$

where λ is the wavelength and φ_k is the initial phase of the kth sensor carrier frequency. It is assumed here that mutual coupling effects among different sensor nodes are negligible.[1] Synchronizing the carriers of the sensor nodes with initial phase $\varphi_k = -\frac{2\pi}{\lambda} d_k(\phi_0)$, we can rewrite the array factor as

$$\begin{aligned} F(\phi/\mathbf{r}, \boldsymbol{\phi}) &= \frac{1}{N} \sum_{k=1}^{N} e^{j\frac{2\pi}{\lambda}[d_k(\phi) - d_k(0)]} \\ &\approx \frac{1}{N} \sum_{k=1}^{N} \exp\left\{ j\frac{2\pi}{\lambda}[-r_k \cos(\phi - \psi_k)] \right\} \\ &= \frac{1}{N} \sum_{k=1}^{N} e^{-j4\pi \tilde{r}_k \sin(\frac{\phi}{2}) \sin(\tilde{\psi}_k)} \\ &= \frac{1}{N} \sum_{k=1}^{N} e^{-j\alpha z_k} \end{aligned} \qquad (2)$$

where $\tilde{r}_k = \frac{r_k}{\lambda}$, $\tilde{\psi}_k = (\psi_k - \frac{\phi}{2})$, $\alpha = \alpha(\phi) = 4\pi \sin(\frac{\phi}{2})$, and the random variable $z_k \triangleq \tilde{r}_k \sin(\tilde{\psi}_k)$ is Gaussian distributed with zero mean and variance $\sigma^2 = \frac{\sigma_0^2}{\lambda^2}$, i.e.,

$$f_{z_k}(z) = \frac{1}{\sqrt{2\pi}\sigma} e^{-\frac{z^2}{2\sigma^2}}, \quad -\infty < z < \infty. \qquad (3)$$

For each realization of $\mathbf{z} = [z_1, z_2, \dots, z_N] \in (-\infty, \infty)^N$, the far-field beampattern can be found as

$$P(\phi/\mathbf{z}) = |F(\phi/\mathbf{z})|^2 = \frac{1}{N} + \frac{1}{N^2} \sum_{k=1}^{N} e^{-j\alpha z_k} \sum_{l=1, l \neq k}^{N} e^{j\alpha z_l}. \qquad (4)$$

B. Average beampattern

The average beampattern is defined as

$$P_{\text{av}}(\phi) = E_z[P(\phi/\mathbf{z})] \qquad (5)$$

where $E_z[\cdot]$ denotes the average over all realizations of z. In the case of Gaussian sensor node distribution, the average beampattern can be derived by substituting (3) and (4) in (5) as

$$P_{\text{av}}(\phi) = \frac{1}{N} + \left(1 - \frac{1}{N}\right) \left| e^{-\frac{\alpha^2 \sigma^2}{2}} \right|^2. \qquad (6)$$

The term $1/N$ in (6) represents the value of the average beampattern in the sidelobe region. It can be seen that the average beampattern has no nulls and no sidelobes. The mainlobe of the average beampattern is represented by the second term in (6), and it decays exponentially with a rate proportional to the variance σ^2. Note that although the average beampattern (6) is similar to the one derived for the case of uniformly distributed

---

[1]Note that mutual coupling does not affect the beampattern, but can cause a power loss for a cluster of WSN. However, the power loss caused by mutual coupling of sensor nodes with low power (that is typically the case for WSN) can be indeed neglected.

sensor nodes [3], in the latter case, the Bessel function of the first kind results also in nulls and sidelobes. The presence of sidelobes in the average beampattern increases the chance of sidelobes with high peaks in a sample beampattern for a specific realization of sensor node locations.

C. The case of truncated Gaussian spatial distribution

For the average beampattern (6), it is assumed that the sensor node spatial distribution has infinite support. However, sensor nodes which are located far away from the cluster center require higher power for communicating with other sensor nodes. Therefore, it might be more practical to neglect these sensor nodes and consider only the sensor nodes inside a disk of radius L. Using the Gaussian spatial distribution (3) where $-L \leq z \leq L$, and equations (4) and (5), the average beampattern can be rewritten as

$$\begin{aligned} P_{\text{av}}(\phi) &= \frac{1}{N} + \frac{1}{N^2} \sum_{k=1}^{N} e^{-\frac{\alpha^2 \sigma^2}{2}} \int_{-L}^{L} \frac{1}{\sqrt{2\pi}\sigma} e^{-\frac{(z_k + j\alpha\sigma^2)^2}{2\sigma^2}} dz_k \\ &\times \sum_{l=1, l \neq k}^{N} e^{-\frac{\alpha^2 \sigma^2}{2}} \int_{-L}^{L} \frac{1}{\sqrt{2\pi}\sigma} e^{-\frac{(z_l - j\alpha\sigma^2)^2}{2\sigma^2}} dz_l. \end{aligned} \qquad (7)$$

Observing that

$$\int_{-L}^{L} \frac{1}{\sqrt{2\pi}\sigma} e^{-\frac{(z + j\alpha\sigma^2)^2}{2\sigma^2}} dz = 1 - 2Q\left(\frac{L + j\alpha\sigma^2}{\sigma}\right) \qquad (8)$$

where $Q(x) = \int_x^\infty \frac{1}{\sqrt{2\pi}\sigma} e^{\frac{t^2}{2\sigma^2}} dt$ is the Q-function, we can rewrite (7) as

$$\begin{aligned} P_{\text{av}}(\phi) &= \frac{1}{N} + \frac{1}{N^2} \left| e^{-\frac{\alpha^2 \sigma^2}{2}} \right|^2 \sum_{k=1}^{N} \left(1 - 2Q\left(\frac{L + j\alpha\sigma^2}{\sigma}\right)\right) \\ &\times \sum_{l=1, l \neq k}^{N} \left(1 - 2Q\left(\frac{L - j\alpha\sigma^2}{\sigma}\right)\right). \end{aligned} \qquad (9)$$

Moreover, applying the Chernoff bound to (9), i.e., using the inequity $Q\left(\frac{L + j\alpha\sigma^2}{\sigma}\right) \leq \frac{1}{2} \exp\left\{-\frac{(L + j\alpha\sigma^2)^2}{2\sigma^2}\right\}$, we obtain that

$$\begin{aligned} P_{\text{av}}(\phi) &\approx \frac{1}{N} + \frac{1}{N^2} \left| e^{-\frac{\alpha^2 \sigma^2}{2}} \right|^2 \sum_{k=1}^{N} \left[1 - e^{-\frac{(L + j\alpha\sigma^2)^2}{2\sigma^2}}\right] \\ &\times \sum_{l=1, l \neq k}^{N} \left[1 - e^{-\frac{(L - j\alpha\sigma^2)^2}{2\sigma^2}}\right] \\ &= \frac{1}{N} + \left(1 - \frac{1}{N}\right) \left| e^{-\frac{\alpha^2 \sigma^2}{2}} \right|^2 \\ &\times \left[1 + e^{-\left(\frac{L}{\sigma}\right)^2} e^{\alpha^2 \sigma^2} - 2e^{-\frac{L^2}{2\sigma^2}} e^{\frac{\alpha^2 \sigma^2}{2}} \cos(L\alpha)\right] \\ &= \frac{1}{N} + \left(1 - \frac{1}{N}\right) e^{-\frac{L^2}{\sigma^2}} + \left(1 - \frac{1}{N}\right) \left| e^{-\frac{\alpha^2 \sigma^2}{2}} \right|^2 \\ &- 2\left(1 - \frac{1}{N}\right) \cos(L\sigma) e^{-\left(\frac{L^2}{2\sigma^2} + \frac{\alpha^2 \sigma^2}{2}\right)}. \end{aligned} \qquad (10)$$

Note that the second term in (10) does not depend on α and, therefore, it only shifts the mean of the average beampattern, while the last term in (10) contributes to the mainlobe. However, for $L \geq 3\sigma$ these two terms are small and can be neglected. It can be seen that the expression

(10) without the second and last terms coincides with the expression (6). Therefore, for our studies it is sufficient to consider only the case of standard Gaussian distribution with infinite support.

Hereafter, when comparing the cases of uniform and Gaussian spatial sensor node distributions, we use $\sigma = \tilde{R}/3$ in the case of Gaussian spatial distribution, where the normalized radius of the cluster $\tilde{R} = R/\lambda$ is defined for uniform distribution [3]. This assumption suggests that in the case of Gaussian distribution, 99.73% of all sensor nodes are located in the disk of radius $\tilde{R}$ and, thus, the sensor nodes' coverage areas in both cases are the same.

D. 3dB beamwidth

The 3dB beamwidth is defined as the angle $\phi_{3\text{dB}}$ at which the power of the average beampattern drops 3dB below the maximum value at $\phi = 0$, i.e., $P_{\text{av}}(\phi_{3\text{dB}}) = \frac{1}{2}$. In the case of Gaussian distributed sensor nodes, the 3dB beamwidth of the average beampattern (6) can be derived as

$$\phi_{3\text{dB}} = 2\sin^{-1}\left(\frac{0.0663}{\sigma}\right) \approx \frac{0.1326}{\sigma}. \quad (11)$$

For the sake of comparison with the case of uniformly distributed sensor nodes, we express (11) in terms of $\tilde{R} = 3\sigma$. Then the expression (11) can be rewritten as

$$\phi_{3\text{dB}} \approx \frac{0.4}{\tilde{R}}. \quad (12)$$

Similar to the case of uniform distribution [3], the 3dB beamwidth in the case of Gaussian spatial sensor node distribution decreases when the cluster radius increases. However, the 3dB beamwidth in the case of Gaussian distributed sensor nodes is larger than in the case of uniform distributed sensor nodes for the same cluster area. The only factor that affect the 3dB beamwidth is the radius $\tilde{R}$. Note that it can often be adjusted at the deployment stage to the desired value.

E. 3dB sidelobe region

The 3dB sidelobe region is the range between the angle ϕ_{Sidelobe} at which the mainlobe of the average beampattern reduces to 3dB above $1/N$ and π, i.e., Sidelobe Region $= \{\phi \mid \phi_{\text{Sidelobe}} \leq |\phi| \leq \pi\}$. In the case of Gaussian distributed sensor nodes, ϕ_{Sidelobe} can be derived by substituting (6) in $P_{\text{av}}(\phi_{\text{Sidelobe}}) = \frac{2}{N}$. After some straightforward manipulations, ϕ_{Sidelobe} can be founded as

$$\phi_{\text{Sidelobe}} = 2\sin^{-1}\left(\frac{\sqrt{\ln(N-1)}}{4\pi\sigma}\right). \quad (13)$$

It can be seen that the sidelobe region depends on the cluster area and the number of sensor nodes N. However, the effect of N is small due to the logarithm and square root operations. Hence, increasing the number of sensor nodes in the case of Gaussian spatial sensor node distribution is not as critical for the sidelobe region as it is in the case of uniform spatial sensor node distribution [3]. Comparing it to the case of uniform distribution, we see that Gaussian distribution produces average beampattern with larger sidelobe region, i.e., the mean of the beampattern is close to $\frac{1}{N}$ over a larger area and, therefore, the sidelobes with high peaks are less probable.

F. Average directivity

The directivity, in the context of WSNs, is changing from one realization of sensor node locations to another. Given a realization of sensor node locations $\mathbf{z}$, the directivity can be expressed as [3]

$$D(\mathbf{z}) = \frac{\int_{-\pi}^{\pi} P(0)d\phi}{\int_{-\pi}^{\pi} P(\phi/\mathbf{z})d\phi} = \frac{2\pi}{\int_{-\pi}^{\pi} P(\phi/\mathbf{z})d\phi} \quad (14)$$

where $P(0) = P(0/\mathbf{z}) = 1$. Then, the average directivity is defined as $D_{\text{av}} = E_z[D(\mathbf{z})]$. The following lower bound on the average directivity is typically considered [3]

$$D_{\text{av}}^* = \frac{2\pi}{\int_{-\pi}^{\pi} P_{\text{av}}(\phi)d\phi}. \quad (15)$$

Using (6) and (15), we can find the lower bound on the average directivity in the case of Gaussian distributed sensor nodes (see Appendix A) as

$$D_{\text{av}}^* = \frac{N}{1 + (N-1)\,_1F_1(\frac{1}{2};1;-(4\pi\sigma)^2)} \quad (16)$$

where $_1F_1(\frac{1}{2};1;-(4\pi\sigma)^2)$ is the hypergeometric function of the first kind.[2] As compared to the case of uniform spatial distribution, the hypergeometric function of the first kind in (16) has larger value than the generalized hypergeometric function $_2F_3(\frac{1}{2},\frac{3}{2};1,2,3;-(4\pi\tilde{R})^2)$ which is used for the case of uniform distribution. Therefore, the average directivity is lower in the case of Gaussian sensor node distribution, as compared to the case of uniform distribution for the same cluster area.

Fig. 1 shows the normalized average directivity D_{av}/N and its normalized lower bound D_{av}^*/N for both uniform and Gaussian spatial distributions. It can be seen that the directivity approaches N asymptotically with increasing the normalized radius $\tilde{R} = 3\sigma$ in both aforementioned cases. Therefore, for a given number of sensor nodes, we can increase the directivity by spreading the sensor nodes over a larger area.

III. RANDOM BEHAVIOR OF THE BEAMPATTERN

In this section, the complementary cumulative distribution function (CCDF) of the beampattern level and the distribution of the maximum sidelobe peak which characterize the random behavior of a sample beampattern, are derived for the case of Gaussian sensor node distribution.

A. Distribution of the beampattern level in the sidelobe region

In order to guarantee that the interference to neighboring clusters is limited, the CCDF of the beampattern level in the sidelobe region should be small enough for any specific realization of sensor node locations. Following [10], the distribution function can be derived by approximating the array factor level at a given angle ϕ using an uncorrelated complex Gaussian random variable with a real part X and an imaginary part Y, that is,

$$F(\phi/\mathbf{z}) = \frac{1}{\sqrt{N}}(X - jY) \quad (17)$$

---

[2]Note that in the case of uniform spatial distribution, the average directivity is represented in terms of the generalized hypergeometric function $_2F_3(\frac{1}{2},\frac{3}{2};1,2,3;-(4\pi\tilde{R})^2)$ instead of $_1F_1(\frac{1}{2};1;-(4\pi\sigma)^2)$.
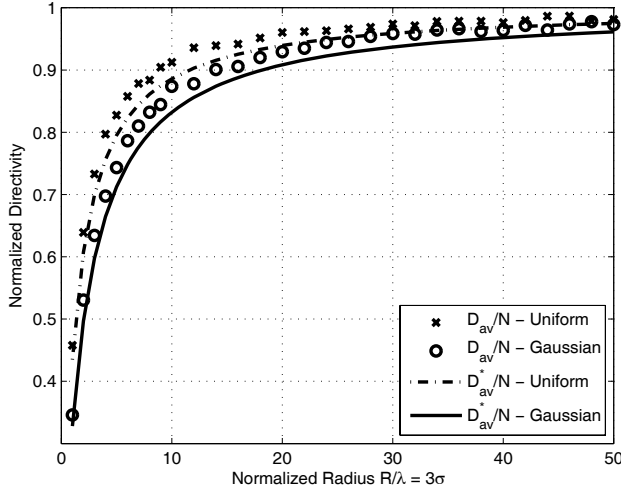
Fig. 1. The normalized directivity $\frac{D_{\mathrm{av}}}{N}$ and the lower bound on the normalized directivity $\frac{D_{\mathrm{av}}^*}{N}$ for both uniform and Gaussian spatial distributions: $N = 16$.

Fig. 2. The mean of the array factor for both uniform and Gaussian spatial distributions: $N = 16, \sigma^2 = 1, \tilde{R} = 3\sigma$.

Fig. 3. The variance of X and Y for both uniform and Gaussian spatial distributions: $N = 16, \sigma^2 = 1, \tilde{R} = 3\sigma$.

where $X = \frac{1}{\sqrt{N}} \sum_{k=1}^{N} \cos(\alpha z_k)$ and $Y = \frac{1}{\sqrt{N}} \sum_{k=1}^{N} \sin(\alpha z_k)$. The joint pdf of X and Y can be written as

$$f_{X,Y}(x,y) = \frac{1}{2\pi\sigma_x\sigma_y} \exp\left[-\frac{|x-m_x|^2}{2\sigma_x^2} - \frac{y^2}{2\sigma_y^2}\right] \quad (18)$$

where the means m_x, m_y and variances σ_x^2, σ_y^2 in the case of Gaussian distributed sensor nodes are derived as $m_x = \sqrt{N}e^{-\frac{\alpha^2\sigma^2}{2}}, \sigma_x^2 = \frac{1}{2}\left(1 + e^{-2\alpha^2\sigma^2}\right) - e^{-\alpha^2\sigma^2}, m_y = 0$, and $\sigma_y^2 = \frac{1}{2}\left(1 - e^{-2\alpha^2\sigma^2}\right)$.

Figs. 2 and 3 show, respectively, the means and the variances of array factor for both uniform and Gaussian spatial distributions. It can be seen that for fixed N the array factor in the case of Gaussian spatial distribution has large mean at the region near to the target direction ($\phi = 0$), and approaching zero with increasing ϕ. Thus, sidelobes of equal level occur with equal probability over whole sidelobe region. In the case of uniform distribution, the mean is oscillating in the sidelobe region and, thus, the probability of high level sidelobes in the beampattern is larger at the angles which correspond to the mean peaks. The variance for both distributions is equal to zero at $\phi = 0$ and increases with the distance from the targeted direction. Therefore, the mainlobe of the sample beampattern matches precisely the mainlobe of the average beampattern, and its behavior can be considered as deterministic. This suggests that the 3dB beamwidth and directivity do not deviated much from the average values and thus the average beampattern is suitable for characterizing the mainlobe of a sample beampattern. Moreover, the variance in the case of Gaussian distribution has lower value than the corresponding value in the case of uniform distribution [3], and thus, the mainlobe is more stable in Gaussian case.

Because of the high value of the variance in the sidelobe region for both Gaussian and uniform pdfs, the shape of a sample beampattern in the sidelobe region completely deviates f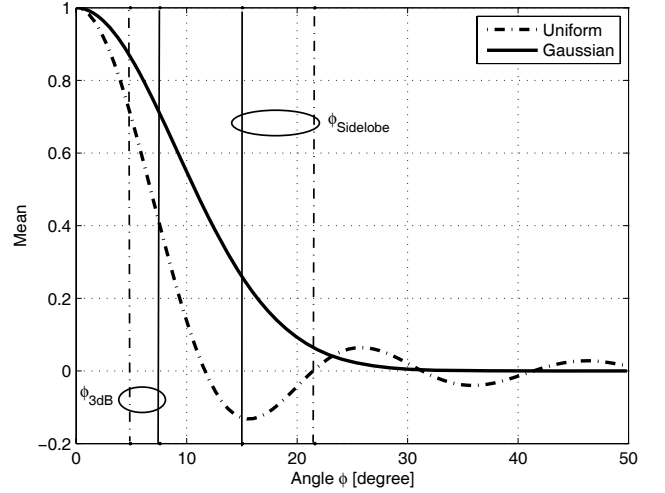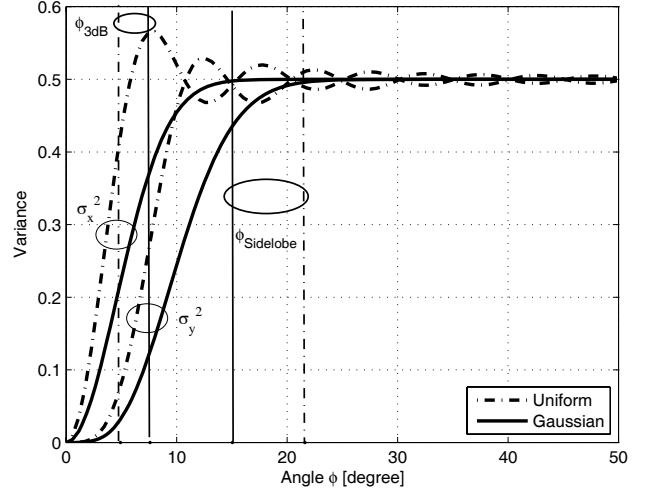rom the shape of the average beampattern. Hence, the average beampattern does not reflect the behavior of a sample beampattern in the sidelobe region, and its characteristics should be expressed in a statistical form.

The CCDF of the beampattern level in the sidelobe region is given as

$$\Pr[P(\phi) > P_0] = \iint_{x^2+y^2>NP_0} f_{X,Y}(x,y)\, dx\, dy$$
$$= \Pr[\sqrt{X^2 + Y^2} > \sqrt{N\, P_0}]. \quad (19)$$

Observing that the variances σ_x^2 and σ_y^2 approach 0.5 in the sidelobe region and thus the beampattern level has Nakagami distribution, the CCDF (19) can be simplified as

$$\Pr[P(\phi) > P_0] = Q_M\left(\frac{m_x}{\sigma_x}, \frac{\sqrt{NP_0}}{\sigma_x}\right)$$
$$= Q_M\left(\sqrt{2}m_x, \sqrt{2NP_0}\right) \quad (20)$$

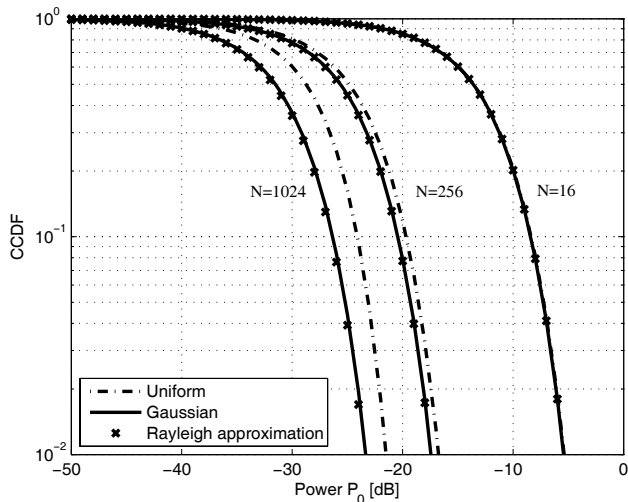where $Q_M(\cdot)$ denotes the first-order Marcum-Q function.

Fig. 4. The CCDF of a sample beampattern for both uniform and Gaussian spatial distributions: $\phi = \frac{\pi}{4}$ and $\tilde{R} = 3\sigma = 2$.
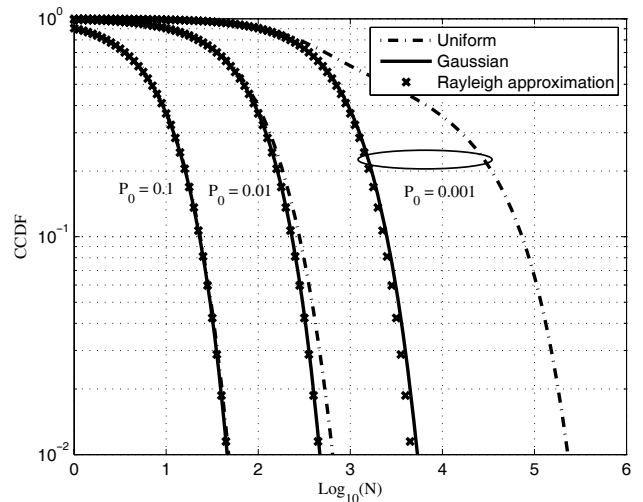

Fig. 5. The CCDF of a sample beampattern as a function of N for both uniform and Gaussian spatial distributions: $\phi = \frac{\pi}{4}$ and $\tilde{R} = 3\sigma = 2$.

Moreover, using the fact that the variances approach equal values, and the mean m_x approaches zero, we can conclude that the beampattern level has Rayleigh distribution and the CCDF can be expressed as

$$\Pr[P(\phi) > P_0] = e^{-NP_0}. \tag{21}$$

This approximation is very accurate in the case of Gaussian distribution for the whole sidelobe region where the array factor has zero mean and the variances are equal to 0.5. However, in the case of uniform distribution, this approximation is valid only for the beampattern nulls and large values of ϕ.

The CCDFs (20) for both uniform and Gaussian sensor node distributions and the Rayleigh approximation to CCDFs (21) are shown in Fig. 4 for N=16, 256, and 1024. It can be seen from the figure that the chance of a high beampattern level in the sidelobe region reduces with increasing the number of sensor nodes N, while this chance is almost independent on the cluster area. The CCDFs for both distributions are the same for low values of N. However, the CCDF in the case of Gaussian distribution is lower than the CCDF in the case of uniform distribution if N is large. The Rayleigh approximation is valid in the case of uniform distribution only if N is small, while it is accurate in the case of Gaussian distribution for any value of N. Fig. 5 shows the CCDF as a function of N for given values of power level P_0. This figure can be used to estimate the number of sensor nodes N required for achieving a certain beampattern level with high probability. It can be seen that for high beampattern levels, both Gaussian and uniform spatial distributions give the same results. However, for low beampattern levels, Gaussian spatial distribution requires less sensor nodes then uniform distribution.

B. Distribution of the maximum sidelobe peak

The probability that the sidelobe with a maximum peak exceeds a given power level is referred hereafter as the outage probability $\Pr_{\text{out}}$ [3]. It can be used to estimate the maximum

possible interference to other clusters in the neighborhood or to estimate the probability of a given interference level to these clusters. An upper bound to the outage probability for the case of Gaussian distributed sensor nodes can be derived similarly to the uniform case [3]. The variances $\sigma_{x'}^2$ and $\sigma_{y'}^2$ can be found as $\sigma_{x'}^2 = \sigma_{y'}^2 = 8\pi^2\sigma^2$, and the average number of upward crossings at a given level a per unit interval du is given as

$$\frac{E[v(a)]}{du} = \frac{a}{2\sqrt{\pi}\pi\sigma} e^{-a^2} \int_0^\infty \omega' e^{-\frac{\omega'^2}{16\pi^2\sigma^2}} d\omega' = 4\sqrt{\pi}\sigma a e^{-a^2}. \tag{22}$$

Integrating (22) over the whole sidelobe region, we obtain that

$$\begin{aligned}
\Pr_{\text{out}} &= E[v(a)] = 2\int_{\phi_{\text{Sidelobe}}}^{\pi} 4\sqrt{\pi}\sigma a e^{-a^2} du \\
&= 8\sqrt{\pi}\left[1 - \sin\left(\frac{\phi_{\text{Sidelobe}}}{2}\right)\right]\sigma a e^{-a^2}. \tag{23}
\end{aligned}$$

Moreover, for low values of ϕ_{Sidelobe}, the upper bound on (23) can be simplified as

$$\Pr_{\text{out}} \le 8\sqrt{\pi}\sigma\sqrt{NP_0} e^{-NP_0}, \quad NP_0 > \frac{1}{2}. \tag{24}$$

The expression (24) shows the relationship between the probability of maximum sidelobe level P_0, the cluster size N, and the cluster area. It can be seen that increasing the cluster area results in higher outage probability, while increasing the cluster size N reduces this probability. Therefore, we can conclude that if the interference is our main concern, it is better to use small size clusters with large number of sensor nodes at each cluster.

Fig. 6 shows the upper bounds on the sidelobe maximum with a given outage probability for both uniform [3] and Gaussian spatial distributions. It can be seen that for the same number of sensor nodes N and outage probability $\Pr_{\text{out}}$, the level of interference to neighboring clusters is lower in the case of Gaussian spatial distribution and the value of the maximum peak in the sidelobe region increases with increasing the normalized radius $\tilde{R} = 3\sigma$.
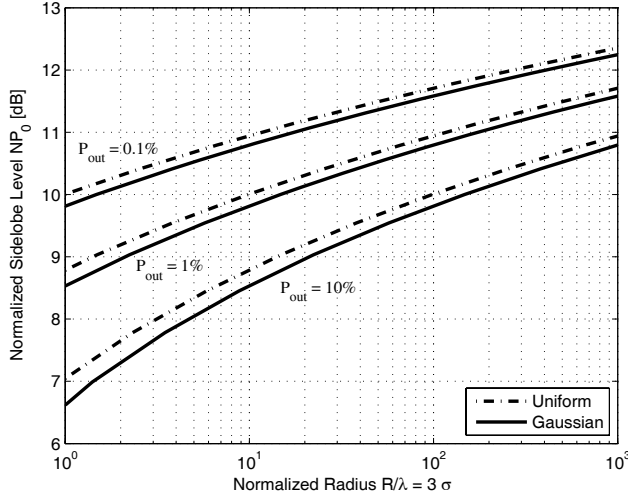
Fig. 6. The upper bound on the sidelobe maximum with a given outage probability $\mathrm{Pr_{out}}$ for both uniform and Gaussian spatial distributions: $N = 16$.

IV. CONCLUSIONS

Gaussian pdf has been proposed as a model for sensor node spatial distribution within a cluster of WSN. The characteristics of the average beampattern have been studied and compared with corresponding characteristics in the case of uniform sensor node spatial distribution. It has been shown that for Gaussian spatial distribution, the beampattern has wider mainlobe and lower chance of large sidelobes as compared to the case of uniform spatial distribution. The outage probability achieves lower value in the case of Gaussian distribution than similar characteristics in the case of uniform distribution. Consequently, it results in smaller interference to the neighboring clusters. Although higher directivity can be achieved if sensor nodes are uniformly distributed, it can be increased simply by spreading the sensor nodes over larger area. The latter can be controlled to some extend at the network deployment stage. The overall conclusion is that the collaborative beamforming provides better performance characteristics when sensor nodes deployment follows Gaussian pdf as compared to the case of uniform pdf, while Gaussian pdf is a realistic model for sensor nodes deployment in wireless applications.

APPENDIX A: DERIVATION OF THE LOWER BOUND ON THE AVERAGE DIRECTIVITY D^*_{av}

Substituting (6) in (15), we obtain the following expression for the lower bound on the average directivity

$$
\begin{aligned}
D^*_{\mathrm{av}} &= \frac{2\,\pi}{\int_{-\pi}^{\pi} \frac{1}{N} + (1 - \frac{1}{N}) \left| e^{\frac{-\alpha(\phi)2\,\sigma^2}{2}} \right|^2 d\phi} \\
&= \frac{2\,\pi\,N}{2\,\pi + (N-1) \int_{-\pi}^{\pi} \left| e^{\frac{-\alpha(\phi)2\,\sigma^2}{2}} \right|^2 d\phi}.
\end{aligned} \quad (25)
$$

The integral in (25) can be found as

$$
\int_{-\pi}^{\pi} \left| e^{\frac{-\alpha(\phi)2\,\sigma^2}{2}} \right|^2 d\phi = \int_{-\pi}^{\pi} e^{-(4\,\pi \sin(\phi/2))^2 \sigma^2} d\phi. \quad (26)
$$

Introducing a new notation $c = (4\pi\sigma)^2$ and changing the variable $u = \sin(\frac{\phi}{2})$, $\frac{du}{d\phi} = \frac{1}{2}\cos(\frac{\phi}{2})$, we can rewrite (26) as

$$
\begin{aligned}
\int_{-1}^{1} e^{-cu^2} \frac{2}{\cos(\frac{\phi}{2})}\,du &= \int_{-1}^{1} e^{-cu^2} \frac{2}{\sqrt{1 - \sin(\frac{\phi}{2})^2}}\,du \\
&= \int_{-1}^{1} e^{-cu^2} \frac{2}{\sqrt{1 - u^2}}\,du. \quad (27)
\end{aligned}
$$

Changing the variable again as $x = u^2$, $\frac{dx}{du} = 2u$, the integral (27) becomes

$$
\begin{aligned}
2\int_{0}^{1} e^{-cx} \frac{2}{\sqrt{1-x}} \frac{1}{2\sqrt{x}} dx &= 2\int_{0}^{1} e^{-cx}(1-x)^{-\frac{1}{2}} x^{-\frac{1}{2}} dx \\
&= 2\pi {}_1F_1\left(\frac{1}{2}; 1; -(4\pi\sigma)^2\right) \quad (28)
\end{aligned}
$$

where $\int_{0}^{1} e^{-cx}(1-x)^{b-a-1} x^{a-1} dx = \frac{\Gamma(b-a)\Gamma(a)}{\Gamma(b)} {}_1F_1(a; b; c)$. Finally, substituting (28) in (25), we obtain (16).

REFERENCES

[1] D. Culler, D. Estrin, and M. Srivastava, "Overview of sensor networks," *IEEE Computer*, pp. 41-49, Aug. 2004.
[2] I. F. Akyildiz, W. Su, Y. Sankarasubramaniam, and E. Cayirci, "A survey on sensor networks," *IEEE Commun. Mag.*, pp. 102-114, Aug. 2002.
[3] H. Ochiai, P. Mitran, H. V. Poor, and V. Tarokh, "Collaborative beamforming for distributed wireless ad hoc sensor networks," *IEEE Trans. Signal Processing*, vol. 53, no. 11, pp. 4110-4124, Nov. 2005.
[4] R. Mudumbai, G. Barriac, and U. Madhow, "On the feasibility of distributed beamforming in wireless networks," *IEEE Trans. Wireless Commun.*, vol. 6, no. 5, pp. 1754-1763, May 2007.
[5] Y. Lo, "A mathematical theory of antenna arrays with randomly spaced elements," *IEEE Trans. Antennas Propagation*, vol. 12, no. 3, pp. 257-268, May 1964.
[6] A. S. Shifrin, *Statistical Antenna Theory*. Golem Press, 1971.
[7] K. Chakrabarty and S. S. Iyengar, *Scalable Infrastructure for Distributed Sensor Networks*. Springer-Verlag, 2005.
[8] J. S. Przemieniecki, *Mathematical Methods in Defense Analyses*. AIAA Education Series, 2000.
[9] D. A. S. Fraser, "Generalized hit probabilities with a Gaussian target," *Ann. Math. Statist.*, vol. 22, no. 2, pp. 248-255, 1951.
[10] M. Donvito and S. Kassam, "Characterization of the random array peak sidelobe," *IEEE Trans. Antennas Propagation*, vol. 27, no. 3, pp. 379-385, May 1979.